The structured core of human β tubulin confers isotype-specific polymerization properties

Melissa C. Pamula, Shih-Chieh Ti, and Tarun M. Kapoor

Laboratory of Chemistry and Cell Biology, The Rockefeller University, New York, NY 10065

Diversity in cytoskeleton organization and function may be achieved through variations in primary sequence of tubulin isotypes. Recently, isotype functional diversity has been linked to a "tubulin code" in which the C-terminal tail, a region of substantial sequence divergence between isotypes, specifies interactions with microtubule-associated proteins. However, it is not known whether residue changes in this region alter microtubule dynamic instability. Here, we examine recombinant tubulin with human β isotype IIB and characterize polymerization dynamics. Microtubules with βIIB have catastrophe frequencies approximately threefold lower than those with isotype βIII, a suppression similar to that achieved by regulatory proteins. Further, we generate chimeric β tubulins with native tail sequences swapped between isotypes. These chimeras have catastrophe frequencies similar to that of the corresponding full-length construct with the same core sequence. Together, our data indicate that residue changes within the conserved β tubulin core are largely responsible for the observed isotype-specific changes in dynamic instability parameters and tune tubulin's polymerization properties across a wide range.

Introduction

Microtubules, polymers of α/β tubulin subunits, carry out a wide range of functions in eukaryotes (Desai and Mitchison, 1997; Nogales, 2001). The tubulin gene family expanded substantially in higher eukaryotes, and the expression of different isotypes can vary according to cell identity and stage of development (Ludueña, 2013). For example, flies encode four α and four β tubulin isotypes, whereas humans encode at least seven α and eight β tubulin isotypes that can have distinct expression profiles (Ludueña and Banerjee, 2008). In particular, βII and βIII are the major β tubulins in the brain (Banerjee et al., 1988), and βVI is limited to the hematopoietic cell lineage (Wang et al., 1986; Leandro-García et al., 2012). Furthermore, recent in vivo studies have revealed that β tubulin isotypes have noninterchangeable roles in development. In *Drosophila melanogaster*, when a testes-specific β tubulin isotype was replaced with a β tubulin isotype not normally expressed in the male germline, axoneme assembly and meiosis were no longer supported (Hoyle and Raff, 1990). In mice, embryonic knockdown of neuronal βIII expression led to neural migration defects that could not be rescued by expression of other β tubulin isotypes (Saillour et al., 2014). Together, these studies suggest that having multiple tubulin isotypes can be important for achieving diversity in function.

Differences in amino acid sequence of tubulin isotypes can affect two important aspects of tubulin function: the binding to microtubule associated proteins (MAPs) and the dynamics of microtubule polymer assembly. Numerous studies examining MAP interactions have focused on the ∼25 amino acids that comprise the C-terminal tail of tubulin, where many posttranslational modifications are found and where isotype sequence differences are concentrated (Westermann and Weber, 2003; Verhey and Gaertig, 2007). Thus it has been proposed that tubulin's C-terminal tail may establish a "tubulin code" to direct unique interactions with MAPs (Verhey and Gaertig, 2007). In contrast, it is unclear whether residue changes in tubulin's C-terminal tail sequence can directly affect microtubule polymerization dynamics. Studies using native tubulin isolated from bovine brain have shown that α/β tubulin dimers with different β isotype composition have distinct polymerization properties (Banerjee et al., 1992; Lu and Ludueña, 1994; Panda et al., 1994), which are partially altered after limited proteolysis by subtilisin (Lu and Ludueña, 1994). However, because of challenges in generating human tubulins with modified amino acid sequence from recombinant sources, the basis of the observed changes in polymerization dynamics between tubulin isotypes is still unknown.

Here, we purify recombinant tubulin heterodimers that have human β tubulin isotype IIB (βIIB) and provide the first characterization of its biochemical properties and assembly dynamics. We quantify parameters of dynamic instability and compare them to those of isotype III (βIII) heterodimers that we have recently examined (Ti et al., 2016). Further, we generate chimeric tail-swapped tubulins by fusing the C-terminal

The Rockefeller University Press $30.00
J. Cell Biol. Vol. 213 No. 4   425–433
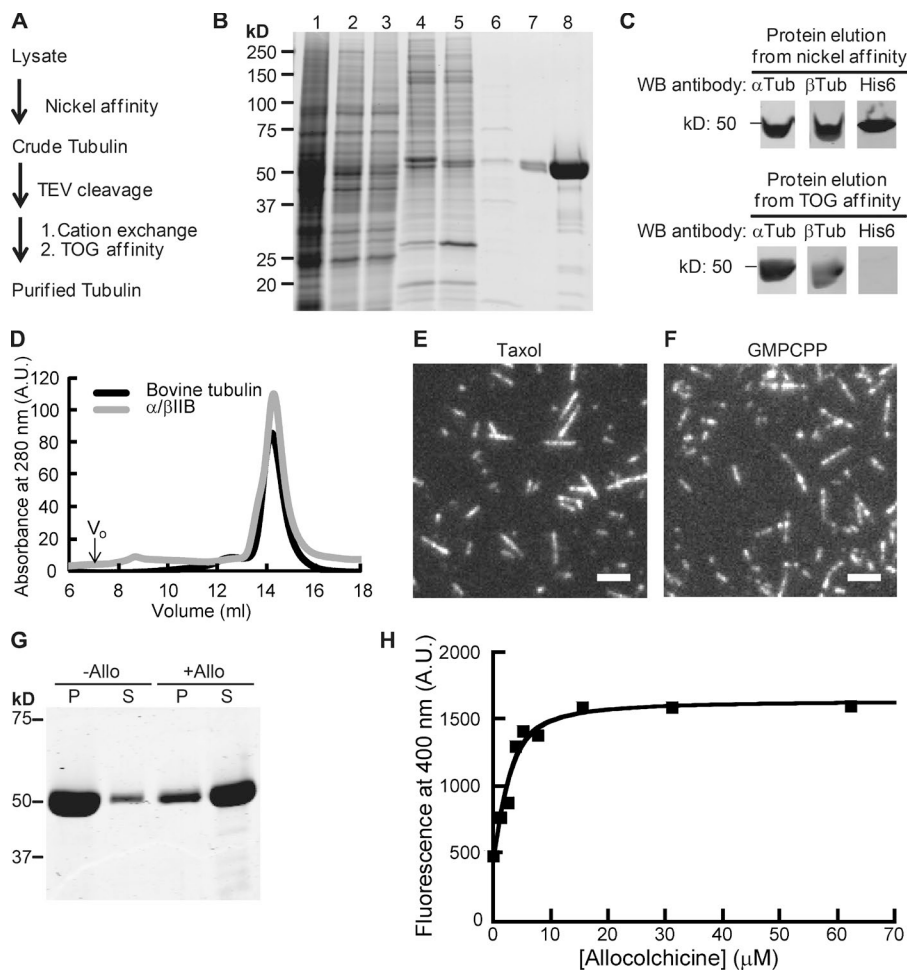www.jcb.org/cgi/doi/10.1083/jcb.201603050

JCB   425

Figure 1. **Purification of recombinant α/βIIB tubulin heterodimers.** (A) Purification scheme. (B) SDS-PAGE analysis (1, lysate; 2, supernatant; 3 and 4, nickel affinity: flow-through (3); elution (4); 5, TEV-digested protein elution from nickel affinity column (a band corresponding to the added TEV protein is at ~25 kD); 6–8, TOG affinity: flow-through (6); elution (7), 20× amount in lane 7 (8); Coomassie stain). (C) Western blot (WB) analyses. Full blots are provided in Fig. S1 A. (D) Elution profiles from size-exclusion chromatography. Peak volume: 14.4 ml (α/βIIB); 14.3 ml (bovine tubulin, used as reference). Void volume (V_0) is 7 ml. A.U., arbitrary units. (E and F) TIRF images of taxol-stabilized (E) or GMPCPP (F) microtubules. Bars, 3 µm. (G) SDS-PAGE analysis of tubulin sedimentation in the presence of allocolchicine (+Allo) or 3% DMSO control (−Allo). Pellet (P) and supernatant (S) fractions are indicated. (H) Representative equilibrium binding curve for α/βIIB with allocolchicine from one experiment is shown. K_d = 1.8 ± 0.42 µM (n = 3, mean ± SD). Fig. S1 C shows data averaged from all three experiments and fitted to a single curve.

tail domain of one isotype to the core of the other and use these proteins to dissect the basis of isotype-specific changes in dynamic instability.

Results and discussion

Purification of recombinant α/βIIB tubulin heterodimers

To determine the biochemical and polymerization properties of human β tubulin isotypes, we purified recombinant tubulin heterodimers using a protocol we have recently developed (Ti et al., 2016). This three-step procedure generated affinity tag–free recombinant protein (Fig. 1, A–C; and Fig. S1 A). We then used mass spectrometry to confirm the presence of human βIIB and showed that heterodimers contained an approximately equimolar mixture of human and insect α tubulins that are ~97% identical by sequence (Fig. S1 B). Efforts to tag both α and β tubulin with different affinity tags led to a substantially reduced protein yield, and the strategy was not pursued further. We find our multistep approach suitable for comparing tubulins with different β isotype compositions, as done in this study. Hereafter, we refer to the purified recombinant tubulin as α/βIIB, highlighting the specific purified human β tubulin isotype.

We assessed the recombinant α/βIIB tubulin using two approaches. First, size-exclusion chromatography indicated that α/βIIB existed as a stable dimer in solution (Fig. 1 D) and eluted at a similar volume to bovine tubulin purified using standard

methods (Al-Bassam et al., 2006; Gell et al., 2011). Second, we examined α/βIIB in the presence of compounds that stabilize or destabilize microtubules. We found that the protein polymerized to form microtubules in the presence of the drug taxol (Fig. 1 E) and the slowly hydrolyzing GTP analogue, GMPCPP (Fig. 1 F). Colchicine and related analogues bind soluble tubulin at an interface between the α and β subunits and inhibit tubulin polymerization (Ravelli et al., 2004). In particular, we examined the binding of our recombinant α/βIIB protein to a colchicine analogue, allocolchicine, which fluoresces only upon binding soluble tubulin and allows for a direct readout of the interaction (Hastie, 1989; Medrano et al., 1989). We first confirmed that allocolchicine can inhibit the assembly of α/βIIB microtubules (Fig. 1 G). We next determined equilibrium binding and found that α/βIIB tubulin binds allocolchicine with a low-micromolar affinity (K_d = 1.8 ± 0.42 µM, n = 3; Figs. 1 H and S1 C), similar to that reported for bovine brain tubulin (Rice et al., 2008). Together, these data indicate that our recombinant α/βIIB protein has overall properties similar to those of bovine tubulin purified using conventional methods.

Polymerization properties of recombinant α/βIIB tubulin heterodimers

To analyze polymerization dynamics of recombinant α/βIIB, we used a total internal reflection fluorescence (TIRF)-based single-filament assay (Fig. 2 A). As a template for microtubule formation, we used GMPCPP-stabilized seeds assembled from α/βIIB tubulin. We then applied solutions of soluble tubulin
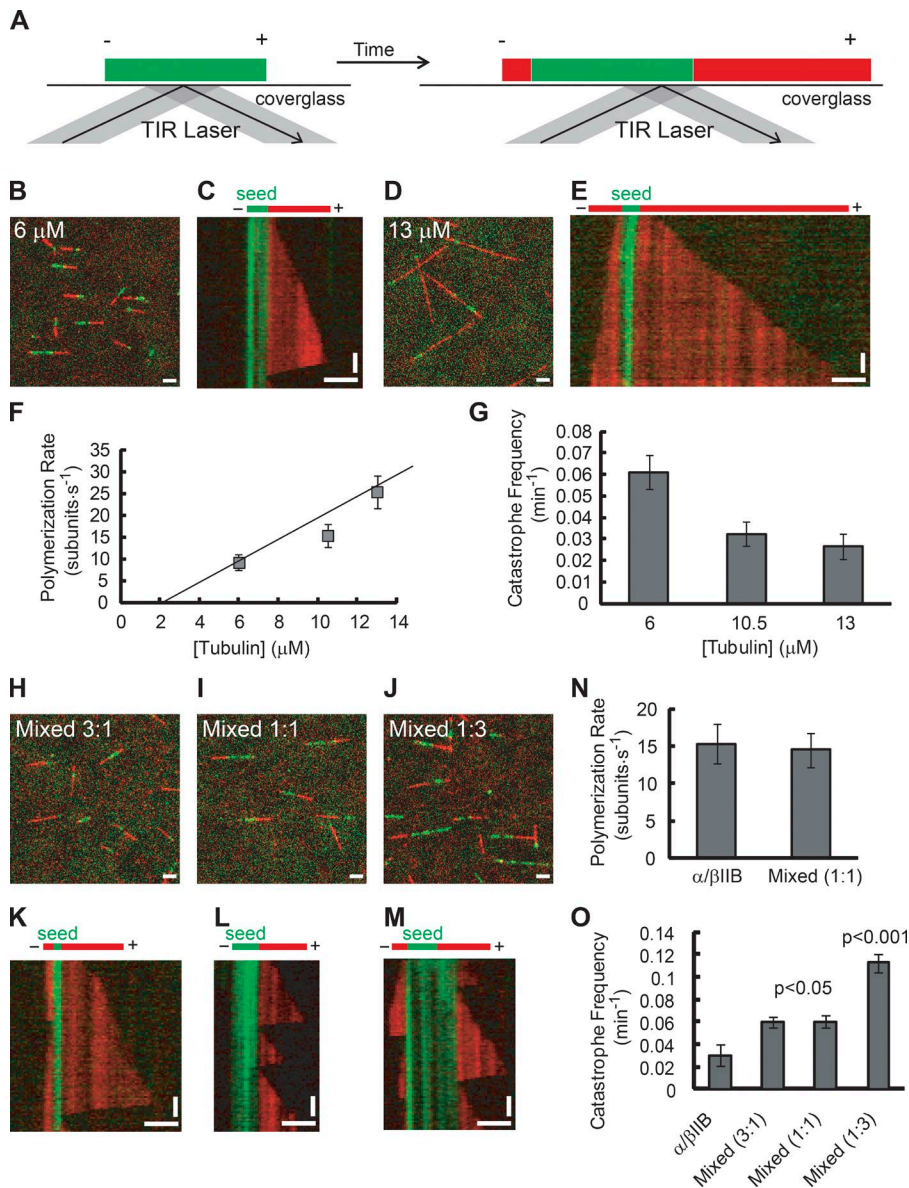
Figure 2. Single-filament TIRF analysis of α/βIIB tubulin polymerization properties. (A) TIRF assay schematic. Microtubule extensions (red) and GMPCPP seeds (green) are shown with plus ends (+) and minus ends (−) indicated. TIRF image overlays (B and D) and kymographs (C and E) of microtubule extensions (red) growing from seeds (green; total tubulin: 6 µM [B and C] and 13 µM [D and E]). (F and G) Plus-end polymerization rates (F) and catastrophe frequencies (G) for microtubules composed of α/βIIB at different total tubulin concentrations. The data were pooled from at least three independent experiments. Overlay images (H–J) and kymographs (K–M) of mixed α/βIIB and α/βIII microtubules (α/βIIB:α/βIII ratio, 3:1 [H and K], 1:1 [I and L], or 1:3 [J and M]; total tubulin, 10.5 µM). (N and O) Plus-end polymerization rate (N) and catastrophe frequency (O) for mixed microtubules (α/βIIB:α/βIII ratio, 1:1, total tubulin, 10.5 µM) with α/βIIB shown for reference. The data were pooled from at least two independent experiments. Bars: (horizontal) 3 µm; (vertical) 2 min. Error bars are SD. For catastrophe frequency (f_{cat}), SD were calculated as $f_{cat}/\sqrt{n}$ (assuming a Poisson distribution), where n is the number of catastrophe events. Table 1 summarizes these measurements.

and observed microtubule assembly off of these seeds over a range of tubulin concentrations (Fig. 2, B and D). To quantify dynamic instability parameters, we generated kymographs from the time-lapse images of growing microtubules (Fig. 2, C and E). Even at the lowest tubulin concentration used (6 µM), we observed growth off of all filaments examined. Microtubule elongation occured primarily at only one end of the seed, which we designate the plus end. In contrast, assembly of microtubule polymer was rarely observed off of the minus ends at this concentration and only occasionally observed at the highest concentration used (13 µM); therefore, we did not quantify the polymerization properties of tubulin at the minus end.

We determined the mean polymerization rate at plus ends of microtubules assembled from α/βIIB tubulin and found that this rate increased with free tubulin concentration (Fig. 2 F and Table 1). The measured growth rates were close to the reported values for α/βIII (Ti et al., 2016) and purified bovine brain tubulin (Walker et al., 1988). We then fitted the data to a simple 1D model (Oosawa, 1970) whose slope and intercept are the apparent association (k_+) and dissociation ($k_−$) rate constants of tubulin subunits, respectively ($k_+ = 1.9 \pm 0.5$ µM^{-1} s^{-1} and $k_− = 2.6 \pm 4.2$ s^{-1}).

We next measured the frequency of catastrophe, the transition from a state of filament growth to a state of rapid shrinkage. Microtubules assembled from α/βIIB heterodimers underwent a catastrophe event infrequently, and we observed a moderate decrease in catastrophe frequency as tubulin concentration was increased from 6 to 13 µM (Fig. 2 G). We measured a frequency of 0.03 ± 0.006 min^{-1} at a tubulin concentration close to physiologic levels (10.5 µM). We rarely observed rescue events (the transition from rapid shortening to relatively slow growth) under our experimental conditions and did not analyze this parameter. When we compared our analysis of recombinant α/βIIB tubulin with that of recombinant β tubulin isotype 3 (α/βIII; Ti et al., 2016), we observed key differences. Notably, the catastrophe frequency for α/βIIB was 1.5- to 3-fold lower than that of α/βIII at all tubulin concentrations tested (P < 0.02 at each concentration; Ti et al., 2016).

Tubulin in cells is a mixture of multiple isotypes of β tubulin. In particular, bovine brain tubulin has been shown to be

a mixture of at least four β isotypes (β2, β3, β4, and β1 detected at 58%, 25%, 13%, and 3%, respectively; Banerjee et al., 1988). Therefore, we mixed α/βIIB and α/βIII heterodimers and analyzed polymerization dynamics (Fig. 2, H–O). At equal ratios of α/βIIB and α/βIII tubulin (10.5 μM total tubulin), microtubules readily polymerized off of GMPCPP seeds (Fig. 2 I). The polymerization rate of these mixed microtubules (14 ± 2 subunit · s^{-1}) was close to that of α/βIIB microtubules (15 ± 3 subunit · s^{-1}; Fig. 2 N) and α/βIII microtubules (Ti et al., 2016) at the same tubulin concentration. This suggests that the two isotypes can indeed copolymerize. If they did not, the expected polymerization rate would be ~7–8 subunit · s^{-1}, as the effective concentration would be 5.25 μM for each isotype. The catastrophe frequency at filament plus ends was 0.06 ± 0.01 min^{-1} at 10.5 μM total tubulin concentration (Fig. 2 O). This value is intermediate between that for α/βIIB microtubules (0.03 ± 0.01 min^{-1}; Fig. 2 G) and that for α/βIII microtubules (Ti et al., 2016). Together, our data indicate that the dynamics of microtubules assembled from mixed tubulin populations depends on the contribution of each isotype, and that mixing gives a catastrophe frequency intermediate between what is observed for either isotype alone.

Characterization of recombinant tubulins containing human β tubulin chimeras

To examine whether residue changes within tubulin's C-terminal tail, which are proposed to specify interactions with MAPs (Sirajuddin et al., 2014), also confer the observed isotype-specific catastrophe frequencies, we generated chimeric β tubulin constructs with the C-terminal tails swapped (Fig. 3 A). We designated the core region (aa 1–427) to be equal to the length of tubulin protein resolved in a recent structural study (Alushin et al., 2014), and the tail region to be the remaining C-terminal amino acids (aa 428–445 in βIIB and 428–450 in βIII). We coexpressed one of the two chimeric β tubulins fused to a cleavable hexahistidine tag along with human α isotype 1B in insect cells and generated the

following two heterodimers: α/βIIB-tail-III (βIIB core and βIII tail) and α/βIII-tail-IIB (βIII core with βIIB tail; Fig. 3 B).

Using our purification protocol, we generated affinity tag–free recombinant chimeric tubulin heterodimers (Fig. 3, C and D; and Fig. S2 A) that were of similar purity to that of α/βIIB. Size-exclusion chromatography analysis indicated that the α/βIIB-tail-III and α/βIII-tail-IIB proteins existed as stable dimers in solution and eluted at a volume similar to the full-length α/βIIB (Figs. 3 E and 1 D). As with the full-length α/βIIB tubulin, we analyzed the chimeric proteins using a TIRF microscopy–based assay. We showed that both chimeric tubulins assembled readily into microtubules in the presence of taxol (Fig. 3 F) and GMPCPP (Fig. 3 G). These experiments indicated that the chimeric tubulins formed stable dimers and polymerized under standard conditions.

Polymerization properties of recombinant tubulins containing β tubulin chimeras

To determine the intrinsic dynamic properties of recombinant tubulin heterodimers containing chimeric β tubulins, we used the same single-filament TIRF assays used to analyze the full-length α/βIIB construct (Fig. 2 A). We first used GMPCPP-stabilized seeds assembled from α/βIIB-tail-III and applied solutions composed of different concentrations of α/βIIB-tail-III onto the seeds. In separate experiments, we examined growth of α/βIII-tail-IIB tubulin off of α/βIII-tail-IIB seeds.

In the case of α/βIIB-tail-III tubulin, we frequently observed growth at only one of the two ends of the seed (Fig. 4, A–D), as was noted for full-length α/βIIB. At the plus ends, the rate of polymerization for microtubules assembled from α/βIIB-tail-III increased with greater concentrations of free tubulin (Fig. 4 I and Table 1). The apparent k_+ (2.0 ± 0.4 μM^{-1} s^{-1}) and k_- (5.5 ± 2.7 s^{-1}) for α/βIIB-tail-III were close to those measured for α/βIIB and α/βIII (Ti et al., 2016).

In contrast, in a solution of α/βIII-tail-IIB tubulin, assembly frequently occurred off both ends of seeds at all tubulin

Table 1. **Plus end dynamic instability parameters for full-length wild-type tubulins and chimeric tubulins**

Total tubulin concentration and recombinant protein	Polymerization rate (subunit · s^{-1})		Catastrophe frequency (min^{-1})	
	Mean ± SD	n	Mean ± SD	n
6 μM				
α/βIIB	9 ± 2	70	0.06 ± 0.008	60
α/βIIB-tail-III	6 ± 1	87	0.08 ± 0.008	92
α/βIII-tail-IIB	8 ± 2	37	0.12 ± 0.02	58
α/βIII*	8 ± 3	77	0.10 ± 0.01	105
10.5 μM				
α/βIIB	15 ± 3	70	0.03 ± 0.006	33
α/βIIB-tail-III	14 ± 3	81	0.03 ± 0.005	37
α/βIII-tail-IIB	17 ± 2	88	0.10 ± 0.01	115
α/βIII*	16 ± 6	75	0.10 ± 0.01	104
Mixed (3:1) (α/βIIB:α/βIII)	ND		0.05 ± 0.008	41
Mixed (1:1) (α/βIIB:α/βIII)	14 ± 2	79	0.06 ± 0.007	65
Mixed (1:3) (α/βIIB:α/βIII)	ND		0.12 ± 0.009	153
13 μM				
α/βIIB	25 ± 4	52	0.03 ± 0.006	20
α/βIIB-tail-III	21 ± 3	49	0.008 ± 0.003	9
α/βIII-tail-IIB	19 ± 3	53	0.08 ± 0.01	62
α/βIII*	19 ± 4	57	0.09 ± 0.01	68

Measurements are from data presented in Fig. 2 (F, G, N, and O) and Fig. 4 (I and J). Mean ± SD are shown. n represents the number of filaments analyzed (for polymerization rate) or catastrophe events (for catastrophe frequency). *, data from Ti et al. (2016); ND, not determined.
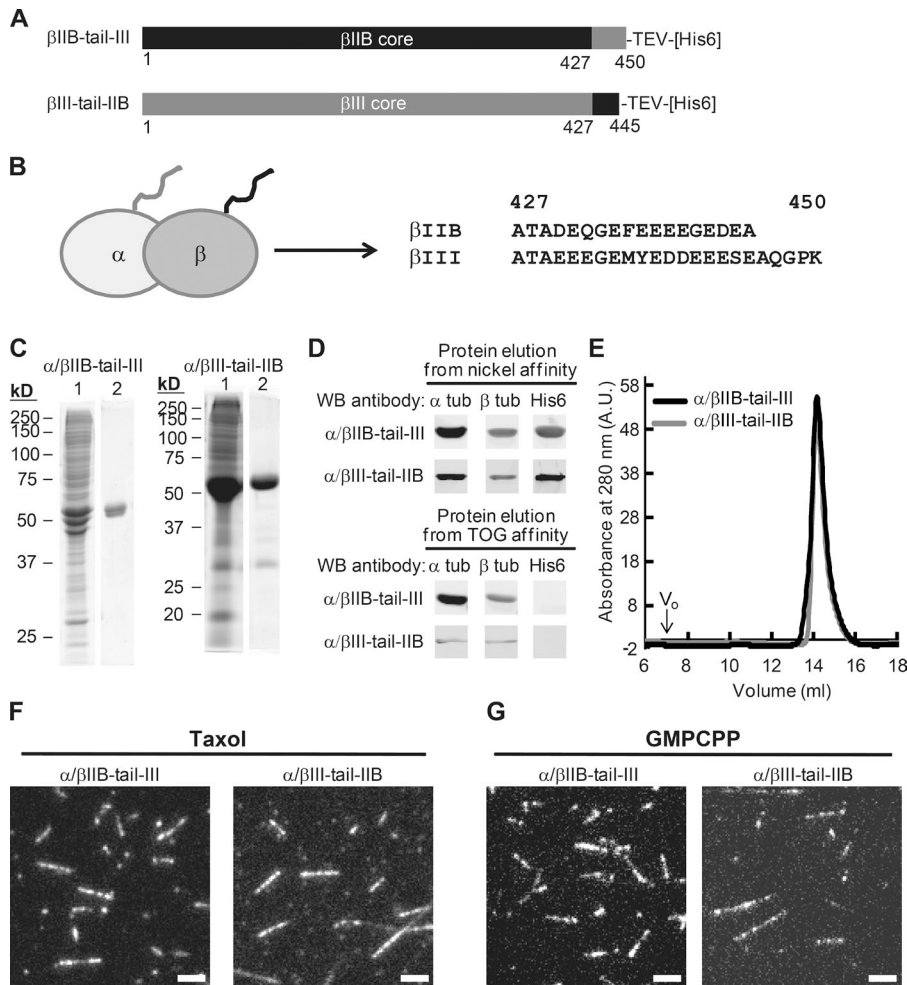
Figure 3. **Design and characterization of chimeric β tubulin constructs.** (A) Design of tail-swapped β tubulin constructs, with amino acid sequence derived from α/βIIB (black) and α/βIII (gray). (B) Schematic of tubulin heterodimer indicating β tubulin C-terminal tail (black). Amino acid sequences from the C terminus of βIIB and βIII are shown. (C) SDS-PAGE analysis (1, nickel affinity elution; 2, TOG affinity elution; Coomassie stain). (D) Western blot (WB) analysis. Full blots are provided in Fig. S2 A. (E) Protein elution profiles from size-exclusion chromatography. Peak volume: 14.2 ml (α/βIIB-tail-III); 14.1 ml (α/βIII-tail-IIB). Void volume (V_0) is 7 ml. A.U., arbitrary units. (F and G) TIRF images of taxol-stabilized (F) or GMPCPP (G) microtubules. Bars, 3 μm.

concentrations (Fig. 4, E–H). This was consistent with what we found for full-length recombinant α/βIII, which grows frequently at both seed ends under similar experimental conditions (Ti et al., 2016). To compare rates between isotypes, we focused on the faster-growing plus end. The polymerization rate of microtubules assembled from α/βIII-tail-IIB tubulin also increased with increasing concentrations of free tubulin (Fig. 4 I). The apparent k_+ (1.8 ± 0.5 μM^{-1} s^{-1}) and k_- (2.4 ± 4.2 s^{-1}) for α/βIII-tail-IIB were close to those of both full-length α/βIIB and full-length α/βIII. These data indicate that each of the chimeric β tubulin constructs can elongate into microtubule polymer at rates close to those measured for each of the full-length wild-type proteins α/βIIB and α/βIII.

We next analyzed catastrophe frequency, the dynamic instability parameter that differs between α/βIIB and α/βIII. For α/βIIB-tail-III microtubules, the catastrophe frequencies were close to those of the full-length α/βIIB at the same tubulin concentrations (Fig. 4 J and Fig. 2 G). Next, we measured the catastrophe frequencies of microtubules assembled from α/βIII-tail-IIB tubulin and found them to be ∼1.5- to 3-fold higher than those of α/βIIB-tail-III microtubules over a range of tubulin concentrations (Fig. 4 J and Table 1). These catastrophe frequencies of α/βIII-tail-IIB microtubules were close to the reported catastrophe frequencies of microtubules assembled from full-length α/βIII (Fig. 4 J and Table 1). Together, these data indicate that the amino acid substitutions within the structured core are crucial for establishing isotype-specific parameters of dynamic instability.

Our studies indicate that microtubules assembled from each of the two tubulin isotypes can have substantially different catastrophe frequencies. The suppression of catastrophe in α/βIIB microtubules observed in vitro is on the order of what can be achieved by regulatory proteins in cells, such as TPX2, and by microtubule-stabilizing drugs, such as taxol (Mohan et al., 2013; Wieczorek et al., 2015). Human tubulins βIIB and βIII differ in amino acid identity at ∼9% of residues within the ∼450-aa polypeptide, and the short ∼25-residue C-terminal tail carries a large fraction (15 of 42) of the total residue changes (Fig. S3 A). Our analyses of chimeric tail-swapped tubulins suggest that of these 42 nonidentical residues, those within the structured core of tubulin are largely responsible for the different dynamics. Recent studies examining the effects of residue mutations in tubulin's intermediate domain (Geyer et al., 2015) and kinesin-binding site (Ti et al., 2016) are beginning to reveal how subtle allostery within the tubulin heterodimer affects microtubule assembly dynamics. Given that there are 27 amino acid differences between the βIIB and βIII isotypes within the tubulin core, and that each may affect long-range communication across the dimer, structure or sequence alone is not likely to help prioritize which residues should be examined. Additional studies will be needed to identify which of the 27 amino acid differences, alone or in combination with other residues, specify the observed differences in dynamic instability. Studies in *Drosophila* have revealed how the exogenous expression of tubulin isotypes from another insect species can alter
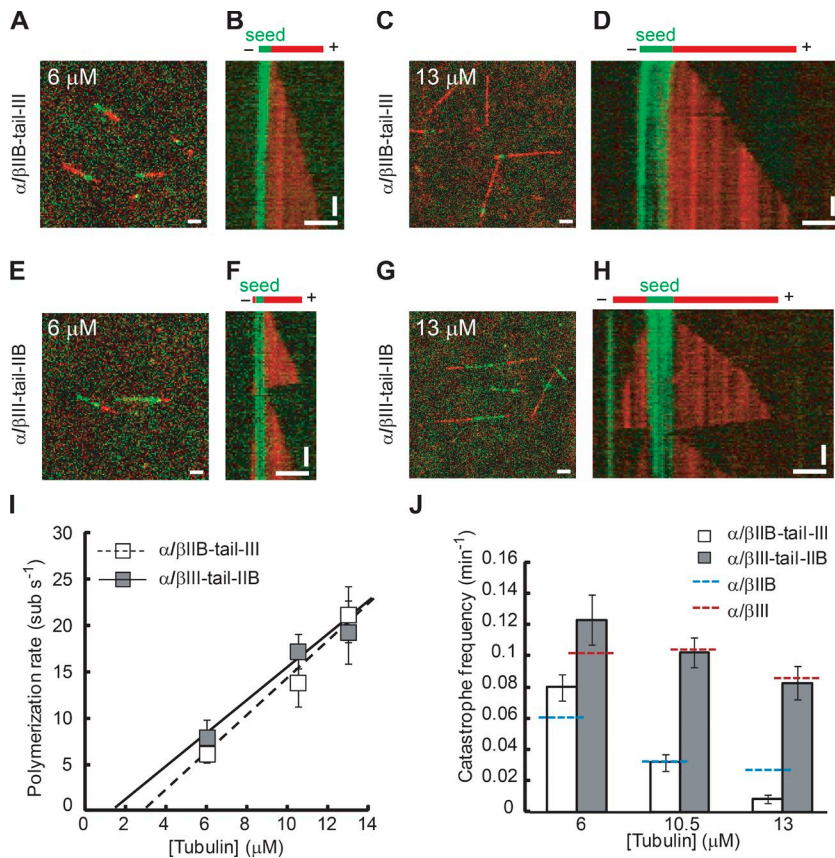
Figure 4. **Single-filament TIRF analysis of chimeric β tubulins.** TIRF image overlays (A, C, E, and G) and kymographs (B, D, F, and H) showing microtubule extensions (red) growing from GMPCPP seeds (green) assembled with α/βIIB-tail-III (A–D) or α/βIII-tail-IIB (E–H). (I and J) Plus-end polymerization rates (I) and catastrophe frequencies (J) for chimeric α/βIIB-tail-III or α/βIII-tail-IIB microtubules at different free tubulin concentrations. Catastrophe frequency measurements for full-length α/βIIB (blue dashed line) and α/βIII (red dashed line) are shown for reference. The data were pooled from at least three independent experiments. Error bars are SD. For catastrophe frequency (f_{cat}), SD were calculated as $f_{cat}/\sqrt{n}$ (assuming a Poisson distribution), where n is the number of catastrophe events. Bars: (horizontal) 3 µm; (vertical) 2 min. Table 1 summarizes these measurements.

microtubule protofilament number in cells (Raff et al., 1997). Our recombinant expression system will help dissect whether these effects are caused by intrinsic properties of tubulin isotypes and whether differences in protofilament number can also regulate dynamic instability.

There are five β tubulins expressed in the brain (Banerjee et al., 1988; Leandro-García et al., 2010). The core sequence of βIIB shares the least amount of similarity with that of βIII compared with the other isotypes expressed in the tissue (Leandro-García et al., 2010; Fig. S2 B). We hypothesize that these two tubulin isotypes establish the range of potential catastrophe frequencies of neuronal microtubules. In addition, our data indicate that recombinant α/βIIB and α/βIII tubulin can copolymerize and form microtubules comprising mixed isotypes, which have catastrophe frequencies intermediate between those measured for microtubules composed of either β tubulin isotype alone. Based on intrinsic polymerization properties alone and a simple model (Verde et al., 1992), the mean length of microtubules assembled from α/βIIB would be approximately three times longer than those assembled from α/βIII (see Materials and methods), and the mean length of mixed microtubules would be intermediate. Thus, microtubule dynamics could be tuned to have different catastrophe frequencies by varying the ratio of different isotypes in cells. Additional functional specialization would come through interactions with MAPs and via posttranslational modifications.

Materials and methods

Purification of recombinant human tubulin

The cDNA encoding *Homo sapiens* α tubulin 1B (NP_006073.2) and β tubulin 2B (BC001352) were cloned into pFastBac Dual vector (Thermo

Fisher Scientific). For affinity purification, a sequence encoding a Tobacco Etch virus (TEV) protease site and hexahistidine tag was fused to the 3′ end of the β tubulin isotype 2B cDNA sequence. We used the Bac-to-Bac system (Thermo Fisher Scientific) to generate recombinant baculovirus. HiveFive cells (Thermo Fisher Scientific), grown to 3.0–3.5 × 10⁶ cells/ml in Sf-900 II SFM (10902-096; Thermo Fisher Scientific) and supplemented with 1× antibiotic-antimycotic (15240-062; Thermo Fisher Scientific), were infected with P3 viral stocks. Cells were cultured in suspension at 27°C and harvested 60 h after infection. The following steps were performed on ice or at 4°C. We lysed cells in an equal volume of lysis buffer (50 mM Hepes, 20 mM imidazole, 100 mM KCl, 1 mM MgCl$_2$, 0.5 mM DTT, 0.1 mM GTP, 3 U/ml benzonase, and 1× protease inhibitor Roche Complete EDTA-free, pH 7.2) by dounce homogenizer (20 strokes) and centrifuged the homogenate at 55,000 rpm in a rotor (Ti70; Beckman Coulter) for 1 h. The supernatant was then filtered through a 0.22-µm Millex-GP PES membrane (SLG-P033RS; EMD Millipore) and loaded at 0.8 ml/min onto a 1-ml HisTrap HP column (17-5247-01; GE Healthcare) preequilibrated with lysis buffer. The column was washed with 25 ml lysis buffer and then eluted with nickel elution buffer (1× BRB80 [80 mM Pipes, 1 mM MgCl$_2$, and 1 mM EGTA], 500 mM imidazole, 0.1 mM GTP, and 1 mM DTT, pH 6.8). The fractions containing proteins were pooled, diluted 10-fold with TOG-column buffer (1× BRB80, 1 mM DTT, and 0.2 mM GTP, pH 6.8), mixed with 6 mg TEV protease, and incubated for 1 h on ice. The TEV-digested protein solution was loaded at 1 ml/min onto tandem chromatography columns consisting of a 1-ml HiTrap SP Sepharose FF column (17-5054-01; GE Healthcare) and a 1-ml TOG-affinity column (Widlund et al., 2012) containing TOG 1 and 2 domains. The columns were then washed with 10 ml TOG column buffer. We removed the 1-ml HiTrap SP Sepharose FF column and washed the 1-ml TOG-affinity column with 20 ml wash buffer 1 (1× BRB80, 1 mM DTT, 0.1 mM GTP, 10 mM MgCl$_2$, and 5 mM ATP, pH 6.8), 20 ml wash buffer 2

(1× BRB80, 1 mM DTT, 0.1 mM GTP, 0.1% Tween-20, and 10% glycerol, pH 6.8), and 10 ml TOG column buffer. The tubulin was eluted with TOG elution buffer (1× BRB80, 500 mM $(NH_4)_2SO_4$, 1 mM DTT, and 0.2 mM GTP, pH 6.8). The eluate containing tubulin was pooled, exchanged into storage buffer (1× BRB80, 5% glycerol, 1 mM DTT, and 0.2 mM GTP, pH 6.8), and concentrated to at least 3 mg/ml with an Amicon Ultra 50K MWCO centrifugal filter (UFC901024; EMD Millipore) within 2 h after elution from the TOG column. A typical preparation yielded 1.5 mg protein from 1 liter of cultured insect cells. The purified tubulin was snap-frozen with liquid nitrogen and stored at −80°C.

Mass spectrometry analysis
Mass spectrometry was performed essentially as described previously (Li et al., 2012). Dried protein samples were resuspended in LDS sample buffer (Thermo Fisher Scientific), reduced, alkylated, and separated on a 4–12% Bis-Tris gradient gel (Thermo Fisher Scientific), followed by in-gel trypsin digestion. Tryptic peptides were purified and analyzed on an LTQ-Orbitrap XL mass spectrometer (Thermo Fisher Scientific). To quantify the relative amounts of human and insect α tubulin in the final protein, we compared the signal intensities for each pair of unique peptides that differed by no more than one amino acid and took the mean for all of the peptide pairs. To examine the possibility of insect β tubulin copurifying in our final protein, we used a similar approach. Insect β tubulin was detected at low abundance, indicating that it is not a major contaminant of our final recombinant protein. We estimate this fraction of insect tubulin to constitute ∼4% of the total β tubulin.

Microtubule sedimentation assay in the presence of allocolchicine
Allocolchicine was synthesized by the established method (Fernholz, 1950). Purified tubulin was preclarified by high-speed centrifugation in a TLA120.1 rotor (Beckman Coulter) at 90,000 rpm for 10 min at 4°C. Solutions of preclarified tubulin (13 µM) were prepared in assay buffer (1× BRB80, 33.33% [vol/vol] glycerol, 1 mM GTP, and 1 mM *tris*(2-carboxyethyl)phosphine [TCEP]) containing 3% DMSO and 60 µM allocolchicine or 3% DMSO alone. The reactions were incubated at RT for 30 min, followed by another 30-min incubation at 37°C, and then subjected to high-speed centrifugation in a TLA 120.1 rotor (Beckman Coulter) at 90,000 rpm for 10 min at 30°C. The supernatant was removed and saved for SDS-PAGE analysis. The pellet was rinsed with 40 µl warm wash buffer (1× BRB80, 60% [vol/vol] glycerol, and 1 mM TCEP) and resuspended in 1× Laemmli sample buffer for SDS-PAGE analysis.

Binding of allocolchicine to tubulin
Purified tubulin was preclarified by high-speed centrifugation in a TLA120.1 rotor (Beckman Coulter) at 90,000 rpm for 10 min at 4°C. Preclarified tubulin (3 µM) was mixed with increasing concentrations of allocolchicine (0, 1.3, 2.6, 3.9, 5.2, 7.8, 15.6, 31.2, or 62.4 µM) in assay buffer (1× BRB80, 5% [vol/vol] glycerol, 1 mM GTP, and 1 mM TCEP). After 2 h of incubation at RT, the emission spectra of the reactions were collected from 360 to 420 nm with 5-nm increments using excitation at 310 nm. The measured fluorescence intensity at 400 nm was plotted on the vertical axis versus allocolchicine concentration on the horizontal axis. To determine the affinity of tubulin for allocolchicine, the unnormalized equilibrium binding curves were fitted with the following equation:

$$\text{Fluorescence intensity at 400 nm} =$$

$$\frac{\left(K_d + [Allo] + [Tubulin]\right) - \sqrt{\left(K_d + [Allo] + [Tubulin]\right)^2 - 4 \times [Allo] \times [Tubulin]}}{2 \times [Tubulin]}$$

$$\times \left(F_{max} - F_{Background}\right) + F_{Background},$$

where K_d represents the dissociation constant for allocolchicine binding, F_{max} represents the fluorescence intensity at plateau, and $F_{background}$ represents the fluorescence intensity of tubulin (62.4 µM) in the absense of allocolchicine.

In vitro fluorescence microscopy
All experiments were performed on an Eclipse Ti microscope (Nikon) equipped with a NA 1.49 100× Plan Apo TIRF objective (Nikon). The microscope setup included a three-axis piezo-electric stage (Nano LP-200; Mad City Labs), an EM-CCD camera (iXon DU-897; Andor Technology), and two-color TIRF imaging optics (lasers: 488 nm [Spectra-Physics] and 561 nm [Cobalt]; filters: emission [FF01-520/35 and FF01-609/54; Semrock], dichroic [Di01-R488/561; Semrock]). Sample chambers were prepared by first cleaning 18 × 18-mm glass coverslips (thickness no. 1; Gold Seal Cover Glass) and 27 × 46-mm slides (40-80000-01; Buehler). To prevent nonspecific surface sticking, we then coated the surface of slides with nonbiotinylated PEG and the surface of coverslips with a mixture of biotinylated PEG and nonbiotinylated PEG according to standard protocols. To build flow chambers, we applied two strips of double-sided tape to a microscope slide and applied the coverslip. Sample chamber volumes were ∼6–8 µl.

To generate seeds for templated microtubule growth, we polymerized the recombinant tubulins at 12-µM concentration along with 8 mol% Alexa Fluor 488 and biotin-labeled bovine tubulin in the presence of 2.5 mM GMPCPP. The polymerized GMPCPP seeds were immobilized on a coverslip by first coating the surface with NeutrAvidin. After a brief incubation with κ-casein to block nonspecific binding to the surface, a mixture of recombinant tubulin and 4 mol% X-rhodamine–labeled bovine tubulin was flowed into the TIRF chamber maintained at 30°C. Time-lapse images were acquired at a rate of one frame every 10 s for 15 min. All assays with dynamic microtubules were done in buffer containing 1× BRB80, 1 mM GTP, 4% glycerol, 0.2 mg/ml κ-casein, 0.2% methylcellulose, and oxygen scavenging mix (25 mM glucose, 40 mg/ml glucose oxidase, 35 mg/ml catalase, and 0.5% β-mercaptoethanol final concentration in reaction).

Image analysis was performed by creating kymographs from the time-lapse TIRF images of microtubules using ImageJ. The data were quantified by measuring the slope of the growing microtubule extension and using it to determine the mean growth speed for each filament. The mean polymerization rate was calculated from all microtubules analyzed for each condition. The mean and standard deviation are reported in the figures. To determine catastrophe frequency, we divided the total number of catastrophe events for all filaments by the total polymerization time (the sum of the time each GMPCPP seed was observed with a growing microtubule extension). The standard deviation was estimated as the catastrophe frequency divided by the square root of the number of catastrophe events. This assumes that catastrophe events are Poisson processes.

Estimating the mean length of microtubules
We used a model that described the probability of finding a microtubule of a given length x at any time, assuming four dynamic instability parameters: v_g (velocity of growth), v_s (velocity of shrinkage), f_{cat} (frequency of catastrophe), and f_{res} (frequency of rescue; Verde et al., 1992).

The length probability distribution can be described as

$$p(x) = \frac{1}{L} \times e^{-\frac{x}{L}}$$

From their derivations, the average length L is estimated by

$$L = \frac{v_s v_g}{(v_s f_{cat}) - (v_g f_{res})}$$

We make the simplifying assumption that $f_{res} = 0$; as we rarely observe rescue events. So this simplifies to

$$L = \frac{v_s v_g}{v_s f_{cat}} = \frac{v_g}{f_{cat}}$$

At 10.5-µM tubulin concentration, the growth rates of α/βIIB microtubules and α/βIII microtubules are approximately equal and the catastrophe frequencies are such that

$$f_{cat\_\alpha/\beta IIB} = \frac{1}{3} f_{cat\_\alpha/\beta III}$$

This implies that the length of α/βIIB microtubules would be approximately threefold greater than that of α/βIII microtubules.

Online supplemental material

Fig. S1 shows the purification of recombinant α/βIIB tubulin heterodimers. Fig. S2 shows the purification of chimeric β tubulin heterodimers and tubulin isotype identity matrix. Fig. S3 shows β tubulin isotypes IIB and III alignment and a secondary structure topology map. Online supplemental material is available at http://www.jcb.org/cgi/content/full/jcb.201603050/DC1.

References

Al-Bassam, J., M. van Breugel, S.C. Harrison, and A. Hyman. 2006. Stu2p binds tubulin and undergoes an open-to-closed conformational change. *J. Cell Biol.* 172:1009–1022. http://dx.doi.org/10.1083/jcb.200511010

Alushin, G.M., G.C. Lander, E.H. Kellogg, R. Zhang, D. Baker, and E. Nogales. 2014. High-resolution microtubule structures reveal the structural transitions in αβ-tubulin upon GTP hydrolysis. *Cell.* 157:1117–1129. http://dx.doi.org/10.1016/j.cell.2014.03.053

Banerjee, A., M.C. Roach, K.A. Wall, M.A. Lopata, D.W. Cleveland, and R.F. Ludueña. 1988. A monoclonal antibody against the type II isotype of beta-tubulin. Preparation of isotypically altered tubulin. *J. Biol. Chem.* 263:3029–3034.

Banerjee, A., M.C. Roach, P. Trcka, and R.F. Ludueña. 1992. Preparation of a monoclonal antibody specific for the class IV isotype of beta-tubulin. Purification and assembly of alpha beta II, alpha beta III, and alpha beta IV tubulin dimers from bovine brain. *J. Biol. Chem.* 267:5625–5630.

Desai, A., and T.J. Mitchison. 1997. Microtubule polymerization dynamics. *Annu. Rev. Cell Dev. Biol.* 13:83–117. http://dx.doi.org/10.1146/annurev.cellbio.13.1.83

Fernholz, H. 1950. Über die Umlagerung des Colchicins mit Natriumalkoholat und die Struktur des Ringes C. *Liebigs Ann. Chem.* 568:63–72. http://dx.doi.org/10.1002/jlac.19505680106

Gell, C., C.T. Friel, B. Borgonovo, D.N. Drechsel, A.A. Hyman, and J. Howard. 2011. Purification of tubulin from porcine brain. *Methods Mol. Biol.* 777:15–28. http://dx.doi.org/10.1007/978-1-61779-252-6_2

Geyer, E.A., A. Burns, B.A. Lalonde, X. Ye, F.A. Piedra, T.C. Huffaker, and L.M. Rice. 2015. A mutation uncouples the tubulin conformational and

GTPase cycles, revealing allosteric control of microtubule dynamics. *eLife.* 4:e10113. http://dx.doi.org/10.7554/eLife.10113

Hastie, S.B. 1989. Spectroscopic and kinetic features of allocolchicine binding to tubulin. *Biochemistry.* 28:7753–7760. http://dx.doi.org/10.1021/bi00445a035

Hoyle, H.D., and E.C. Raff. 1990. Two *Drosophila* beta tubulin isoforms are not functionally equivalent. *J. Cell Biol.* 111:1009–1026. http://dx.doi.org/10.1083/jcb.111.3.1009

Leandro-García, L.J., S. Leskelä, I. Landa, C. Montero-Conde, E. López-Jiménez, R. Letón, A. Cascón, M. Robledo, and C. Rodríguez-Antona. 2010. Tumoral and tissue-specific expression of the major human beta-tubulin isotypes. *Cytoskeleton (Hoboken).* 67:214–223. http://dx.doi.org/10.1002/cm.20436

Leandro-García, L.J., S. Leskelä, L. Inglada-Pérez, I. Landa, A.A. de Cubas, A. Maliszewska, I. Comino-Méndez, R. Letón, Á. Gómez-Graña, R. Torres, et al. 2012. Hematologic β-tubulin VI isoform exhibits genetic variability that influences paclitaxel toxicity. *Cancer Res.* 72:4744–4752. http://dx.doi.org/10.1158/0008-5472.CAN-11-2861

Li, X., E.A. Foley, K.R. Molloy, Y. Li, B.T. Chait, and T.M. Kapoor. 2012. Quantitative chemical proteomics approach to identify post-translational modification-mediated protein-protein interactions. *J. Am. Chem. Soc.* 134:1982–1985. http://dx.doi.org/10.1021/ja210528v

Lu, Q., and R.F. Ludueña. 1994. In vitro analysis of microtubule assembly of isotypically pure tubulin dimers. Intrinsic differences in the assembly properties of alpha beta II, alpha beta III, and alpha beta IV tubulin dimers in the absence of microtubule-associated proteins. *J. Biol. Chem.* 269:2041–2047.

Ludueña, R.F. 2013. A hypothesis on the origin and evolution of tubulin. *Int. Rev. Cell Mol. Biol.* 302:41–185. http://dx.doi.org/10.1016/B978-0-12-407699-0.00002-9

Ludueña, R.F., and A. Banerjee. 2008. The isotypes of tubulin. *In* The Role of Microtubules in Cell Biology, Neurobiology, and Oncology. T. Fojo, editor. Humana Press, New York, NY. 123–175. http://dx.doi.org/10.1007/978-1-59745-336-3_6

Medrano, F.J., J.M. Andreu, M.J. Gorbunoff, and S.N. Timasheff. 1989. Roles of colchicine rings B and C in the binding process to tubulin. *Biochemistry.* 28:5589–5599. http://dx.doi.org/10.1021/bi00439a038

Mohan, R., E.A. Katrukha, H. Doodhi, I. Smal, E. Meijering, L.C. Kapitein, M.O. Steinmetz, and A. Akhmanova. 2013. End-binding proteins sensitize microtubules to the action of microtubule-targeting agents. *Proc. Natl. Acad. Sci. USA.* 110:8900–8905. http://dx.doi.org/10.1073/pnas.1300395110

Nogales, E. 2001. Structural insight into microtubule function. *Annu. Rev. Biophys. Biomol. Struct.* 30:397–420. http://dx.doi.org/10.1146/annurev.biophys.30.1.397

Oosawa, F. 1970. Size distribution of protein polymers. *J. Theor. Biol.* 27:69–86. http://dx.doi.org/10.1016/0022-5193(70)90129-3

Panda, D., H.P. Miller, A. Banerjee, R.F. Ludueña, and L. Wilson. 1994. Microtubule dynamics in vitro are regulated by the tubulin isotype composition. *Proc. Natl. Acad. Sci. USA.* 91:11358–11362. http://dx.doi.org/10.1073/pnas.91.24.11358

Raff, E.C., J.D. Fackenthal, J.A. Hutchens, H.D. Hoyle, and F.R. Turner. 1997. Microtubule architecture specified by a beta-tubulin isoform. *Science.* 275:70–73. http://dx.doi.org/10.1126/science.275.5296.70

Ravelli, R.B., B. Gigant, P.A. Curmi, I. Jourdain, S. Lachkar, A. Sobel, and M. Knossow. 2004. Insight into tubulin regulation from a complex with colchicine and a stathmin-like domain. *Nature.* 428:198–202. http://dx.doi.org/10.1038/nature02393

Rice, L.M., E.A. Montabana, and D.A. Agard. 2008. The lattice as allosteric effector: structural studies of αβ- and γ-tubulin clarify the role of GTP in microtubule assembly. *Proc. Natl. Acad. Sci. USA.* 105:5378–5383. http://dx.doi.org/10.1073/pnas.0801155105

Saillour, Y., L. Broix, E. Bruel-Jungerman, N. Lebrun, G. Muraca, J. Rucci, K. Poirier, R. Belvindrah, F. Francis, and J. Chelly. 2014. Beta tubulin isoforms are not interchangeable for rescuing impaired radial migration due to Tubb3 knockdown. *Hum. Mol. Genet.* 23:1516–1526. http://dx.doi.org/10.1093/hmg/ddt538

Sirajuddin, M., L.M. Rice, and R.D. Vale. 2014. Regulation of microtubule motors by tubulin isotypes and post-translational modifications. *Nat. Cell Biol.* 16:335–344. http://dx.doi.org/10.1038/ncb2920

Ti, S.C., M.C. Pamula, S.C. Howes, C. Duellberg, N.I. Cade, R.E. Kleiner, S. Forth, T. Surrey, E. Nogales, and T.M. Kapoor. 2016. Mutations in human tubulin proximal to the kinesin-binding site alter dynamic instability at microtubule plus- and minus-ends. *Dev. Cell.* 37:72–84. http://dx.doi.org/10.1016/j.devcel.2016.03.003

Verde, F., M. Dogterom, E. Stelzer, E. Karsenti, and S. Leibler. 1992. Control of microtubule dynamics and length by cyclin A- and cyclin B-dependent

kinases in *Xenopus* egg extracts. *J. Cell Biol.* 118:1097–1108. http://dx .doi.org/10.1083/jcb.118.5.1097

Verhey, K.J., and J. Gaertig. 2007. The tubulin code. *Cell Cycle.* 6:2152–2160. http://dx.doi.org/10.4161/cc.6.17.4633

Walker, R.A., E.T. O'Brien, N.K. Pryer, M.F. Soboeiro, W.A. Voter, H.P. Erickson, and E.D. Salmon. 1988. Dynamic instability of individual microtubules analyzed by video light microscopy: rate constants and transition frequencies. *J. Cell Biol.* 107:1437–1448. http://dx.doi.org/10 .1083/jcb.107.4.1437

Wang, D., A. Villasante, S.A. Lewis, and N.J. Cowan. 1986. The mammalian β-tubulin repertoire: hematopoietic expression of a novel, heterologous β-tubulin isotype. *J. Cell Biol.* 103:1903–1910. http://dx.doi.org/10.1083 /jcb.103.5.1903

Westermann, S., and K. Weber. 2003. Post-translational modifications regulate microtubule function. *Nat. Rev. Mol. Cell Biol.* 4:938–947. http://dx.doi .org/10.1038/nrm1260

Widlund, P.O., M. Podolski, S. Reber, J. Alper, M. Storch, A.A. Hyman, J. Howard, and D.N. Drechsel. 2012. One-step purification of assembly-competent tubulin from diverse eukaryotic sources. *Mol. Biol. Cell.* 23:4393–4401. http://dx.doi.org/10.1091/mbc.E12-06-0444

Wieczorek, M., S. Bechstedt, S. Chaaban, and G.J. Brouhard. 2015. Microtubule-associated proteins control the kinetics of microtubule nucleation. *Nat. Cell Biol.* 17:907–916. http://dx.doi.org/10.1038/ncb3188